Quasi-Elastic Electron-Deuteron Scattering and Neutron Form Factors*

J. R. DUNNING, JR., K. W. CHEN,† A. A. CONE, G. HARTWIG,‡ N. F. RAMSEY, J. K. WALKER, AND RICHARD WILSON
Harvard University, Cambridge, Massachusetts

(Received 9 June 1965; revised manuscript received 8 September 1965)

The cross section for inelastic electron-deuteron scattering has been measured in the four-momentum transfer region corresponding to $q^2=0.389$ to 6.81 $(\mathrm{BeV}/c)^2$ ($q^2=10$ to 175 F^2). The impulse approximation was used in the form given by Durand to interpret the deuteron cross sections as the sum of free-proton and free-neutron scattering cross sections. Using elastic electron-proton scattering cross sections obtained with a hydrogen target and using the Rosenbluth equation, neutron form factors were obtained at $q^2=0.389$, 0.623, 0.857, 1.17, and 1.75 $(\mathrm{BeV}/c)^2$. Upper limits on the form factors were extracted from the $q^2=2.92$, 3.89, and 6.81 $(\mathrm{BeV}/c)^2$ data. No evidence for possible core terms was found in either form factor.

I. INTRODUCTION

THIS paper is concerned with measurements of the electromagnetic structure of the neutron. The 6-BeV internal beam of the Cambridge Electron Accelerator and a liquid-deuterium target have been used to investigate quasielastic electron-deuteron scattering in a range of q^2 to the nucleon varying from 0.389 to 6.89 $(\mathrm{BeV}/c)^2$ (10 to 175 F^{-2}). The scattered electrons were detected with a spectrometer of 6.94% momentum acceptance. The quasi-elastic recoil protons were also detected at $q^2=0.389$ to 1.17 $(\mathrm{BeV}/c)^2$ and the forward scattering angles. Here the ratio of neutron-to-proton scattering was obtained in a single measurement. The 31° laboratory scattering angles employed in part of the present experiment provide enhanced sensitivity to the neutron's charge form factor. These data and the electron-proton scattering data presented in the preceding paper[1] (hereafter called I) were obtained concurrently. They considerably extend the range of four-momentum transfer $[\sqrt{(q^2)}]$ studied experimentally.

Other measurements of quasi-elastic scattering from the deuteron have been made most recently by Hughes *et al.* at Stanford[2] and by Akerlof *et al.* at Cornell.[3] These have extended up to $q^2=1.36$ $(\mathrm{BeV}/c)^2$. At Stanford the cross section for the recoil electron, $d^2\sigma_D/d\Omega dE_3$, was measured at the quasi-elastic peak. The electron-neutron scattering cross section was calculated from the data using a separate measurement of the e-p scattering cross section and what amounts to a subtraction technique. The Cornell data were interpreted in a manner similar to the noncoincidence data of the present paper. The momentum acceptance of their spectrometer was sufficiently large so that an integral over the quasi-elastic scattering cross section was measured. The impulse approximation was used to calculate the fraction of quasi-elastic events outside of this momentum acceptance. A separate measurement of the electron-proton scattering cross section was also necessary. In both these experiments, the ratio $S=\sigma_{en}/\sigma_{ep}$ had fewer systematic uncertainties associated with it than the individual cross section. This ratio was in all cases measured to be less than one. Two statistically independent measurements must be subtracted to obtain S and the error on the ratio is worse than the error on one measurement by a factor of 3 to 4. The magnetic form factor G_{Mn} dominated the scattering and the square of the electric form factor $G_{En}{}^2$ was measured to be consistent with zero or even negative.

These electron-neutron scattering results were less extensive and of lesser precision than comparable proton data. The lack of a free-neutron target has considerably complicated analysis.

One approach to avoiding the large error has been the coincidence method of Stein *et al.* at Cornell.[4] They measure directly the ratio of high-energy protons to neutrons associated with a quasi-elastic recoil electron. Previous data have been reported at $q^2=0.2$ $(\mathrm{BeV}/c)^2$.

Experiments directly sensitive to the charge form factor have been undertaken using thermal neutrons. The quantity derived from thermal-neutron data is (dG_{En}/dq^2) at $q^2=0$. A weighted average of the measurements of Melkonian *et al.*[5] and earlier less precise results yield

$$\left.\frac{dG_{En}}{dq^2}\right|_{q^2=0}=+0.022(1\pm0.031)\mathrm{F}^2=+0.564\ (\mathrm{BeV}/c)^{-2}. \tag{1}$$

Within errors, the entire effect is accounted for through the interaction between the electron and the neutron's magnetic moment: $-G_{Mn}(0)/4M^2$. This result together

* This work supported by the U. S. Atomic Energy Commission.

† Present address: Palmer Physical Laboratory, Princeton University and Princeton-Pennsylvania Accelerator, Princeton, New Jersey.

‡ Present address: Institute für Experimentalle Kernphysik, Karlsruhe, Germany.

[1] K. W. Chen, A. A. Cone, J. R. Dunning, Jr., N. F. Ramsey, J. K. Walker, and Richard Wilson, preceding paper, Phys. Rev. **140**, B1267 (1965). A preliminary account of these measurements appeared in Phys. Rev. Letters **13**, 631 (1964).

[2] E. B. Hughes, T. A. Griffy, M. R. Yearian, and R. Hofstadter, Phys. Rev. **139**, B458 (1965).

[3] C. W. Akerlof, K. Berkelman, G. Rouse, and M. Tigner, Phys. Rev. **135**, B810 (1964).

[4] P. Stein, R. W. McAllister, B. D. McDaniel, and W. M. Woodward, Phys. Rev. Letters **9**, 403 (1962) and (private communication).

[5] E. Melkonian, B. M. Rustad, and W. W. Havens, Jr., Phys. Rev. **114**, 1571 (1959).

with the known zero value of the neutron's charge $[G_{En}(0)=0]$ have led to the speculation that[6]

$$G_{En}(q^2)=(-q^2/4M^2)G_{Mn}(q^2). \quad (2)$$

On the other hand, the precise elastic e-D scattering measurements of Drickey and Hand[7] and Benaksas *et al.*[8] yield the experimentally precise result

$$G_{En}=0.00\pm0.02 \text{ out to } 0.2 \text{ (BeV/}c\text{)}^2. \quad (3)$$

They measure the quantity $G_E=G_{Ed}(G_{En}+G_{Ep})$, and G_{Ed} must be calculated from a theory of the deuteron. These two classes of experiment are inconsistent.

A third approach to obtaining G_{En} is through precise quasi-elastic electron-deuteron scattering-cross-section measurements. The theoretical ambiguities involved here are less important than those arising in elastic electron-deuteron scattering. In addition to the electric form factors G_{En}, magnetic form factors G_{Mn} can also be obtained.

The present experiment measured the quasi-elastic electron scattering from the deuteron. Two experimental methods were employed to extract the electron-neutron scattering cross section and to minimize theoretical ambiguities. First, only the scattered electron was detected. This is called the "electron-detection method" and is described in Sec. II. In the second method a coincidence was demanded between a high-energy recoil proton and the scattered electron. This approach is called the "anticoincidence method." It is capable of much higher experimental precision than was achieved in the present study. This method is discussed in Sec. III. The deuteron model and computational techniques we used to extract the neutron cross sections are presented in detail in Appendix I. The present paper describes the experimental techniques used to obtain electron-neutron scattering cross sections. Attempts to understand these data and the electron-proton scattering results are presented in an accompanying paper.

II. ELECTRON-DETECTION METHOD

At all momentum transfers studied, the scattered electron momentum spectrum was measured with deuterium in the target. The target and beam-monitoring procedures are described in detail in Paper I. The spectrometer used for electron detection was the same as that used in I. Here, the electron spectrometer momentum acceptance of 6.94% was centered on the quasi-elastic peak. A separate measurement was made with hydrogen in the target. The ratio S, was calculated using

$$S=\sigma_{en}/\sigma_{ep}=[\sigma_{ed}/(1+\Delta)-\sigma_{ep}]/\sigma_{ep}. \quad (4)$$

The quantity σ_{ed} is proportional to the total number of events scattered quasi-elastically. To obtain σ_{ed} from

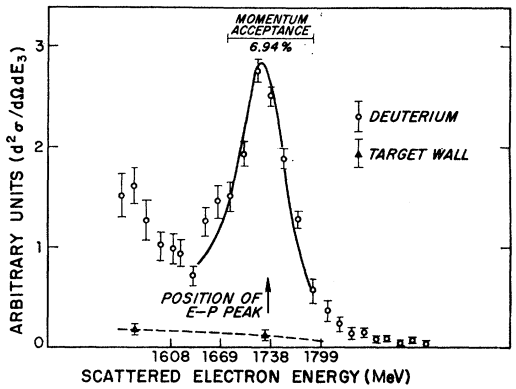

FIG. 1. Inelastic electron momentum spectrum from deuterium at $q^2=1.17$ (BeV/c)^2 and 31°. The line represents Eq. (A1) with radiative corrections included. This curve was normalized to give the best fit.

the observed cross section a correction was made for the fraction of events scattered quasi-elastically but outside the momentum acceptance of the spectrometer. This correction was calculated using the impulse approximation as applied by Durand,[9] radiative corrections of Meister and Griffy,[10] and the final-state corrections of Nuttall and Whippman,[11] wherever applicable. This analysis is discussed in the Appendix.

Precise knowledge of the shape of the momentum acceptance of the spectrometer is necessary to apply this method. The observed elastic electron-proton scattering momentum spectrum was used as a calibration. This momentum spectrum was measured with the finer 1.1% momentum counters labeled 3 to 7 in Fig. 2 of Paper I. The apparent momentum broadening due to these counters was removed. The resultant spectrum was folded into the momentum acceptance to be expected from the counters C_2 and C_8 (see Fig. 2 of I), a point target, and the trajectories of particles passing through the center of the angular acceptance. This procedure compensates for the actual target size, the number of traversals of the incident beam, aberrations near the edge of the quadrupole field, and small misalignment errors. As explained in I, the vertical illumination of the target was not easily measured and it depended on the incident energy. A momentum acceptance was also computed from the nominal target dimensions, and calculated aberrations. In practice, the difference between these two momentum acceptances resulted in altering the fraction of the quasi-elastic peak accepted by the spectrometer by 3% at 30° and 5% at 90°. The experimental numbers were used and an error equal to one-half of the difference assigned.

Typical electron momentum spectra from deuterium are shown in Figs. 1, 2, and 3. The expected shape of the quasi-elastic spectrum is shown for reference. All events

[6] L. N. Hand, D. G. Miller, and R Wilson, Rev Mod. Phys. 35, 335 (1963).
[7] D. Drickey and L. N. Hand, Phys. Rev. Letters 9, 521 (1962).
[8] D. Benaksas, D. Drickey, and D. Frèrejacque, Phys. Rev. Letters 13, 353 (1964).
[9] L. Durand, Phys. Rev. 123, 1393 (1961).
[10] N. T. Meister and T. A. Griffy, Phys. Rev. 133, B1032 (1964).
[11] J. Nuttall and M. L. Whippman, Phys. Rev. 130, 2495 (1963). Note these apply only to the quasi-elastic peak.

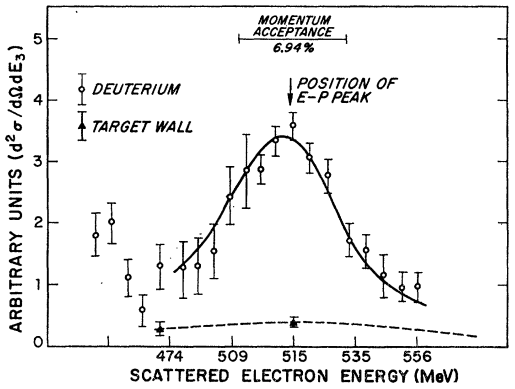

FIG. 2. Inelastic electron momentum spectrum from deuterium $q^2=1.17$ (BeV/c)^2 and $\theta=90°$.

have the signature of electrons. A comparison between Figs. 1 and 3 shows that significant electron contamination was in some cases present from inelastic events where one or more pions were produced. At $q^2=2.92$ (BeV/c)^2 the quasielastic peak appears only as a "shoulder" on this inelastic continuum. To estimate this contamination the measured inelastic spectrum with hydrogen in the target was used. The expected momentum spread due to the deuteron wave function was combined with this hydrogen spectrum. The resultant spectrum shape was normalized to the inelastic electron spectrum from deuterium at the momentum corresponding to the $\frac{3}{2}$, $\frac{3}{2}$ resonance. The process is shown graphically in Fig. 4. The quasi-elastic radiative tail was taken into account. The inelastic electron contaminations estimated in this manner are listed in Table I.

These backgrounds limit the accuracy of the quasi-elastic scattering method. At $q^2=3.89$ (BeV/c)^2 we choose to leave this contamination in the data. The numbers we present at that q^2 are upper limits on R.

All data used to calculate S were obtained as absolute cross sections from the 6.94% momentum acceptance. The 1.1% momentum counters served as an additional check.

Data were reduced using the spectrum of pulse heights from the shower counter C_{11}. The nonelectromagnetic

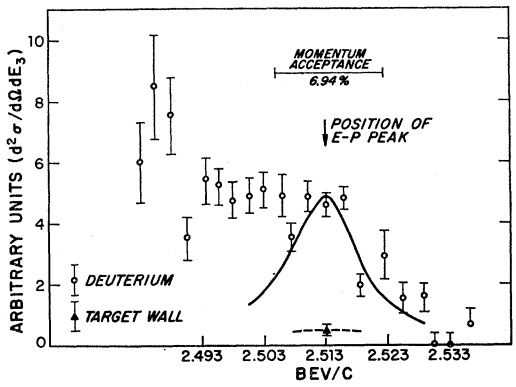

FIG. 3. Inelastic electron momentum spectrum from deuterium $q^2=2.92$ (BeV/c)^2 and $\theta=31°$.

TABLE I. Inelastic electron contamination to quasi-elastic peak.[a]

q^2 (BeV/c)^2	31°	90°
1.17	0.000±0.005	...
1.75	0.037±0.01	0.011
2.92	0.112±0.035	...
3.89	0.18 ±0.085	...

[a] All are fractional contaminations.

background was monitored by placing a 2.8-radiation-length lead sheet between the target and the spectrometer and observing the spectrum of remaining pulses from the shower counter. At the 31° scattering angle this contamination was reduced to negligible proportions by the Čerenkov gas counter. At the 90° scattering angle, significant single-particle pulse-height maxima were observed in the shower spectra with deuterium in the target.

Where this contamination was observed, a high bias in the shower counter was used to improve the rejection of these events. At $q^2=1.75$ (BeV/c)^2 and 90°, 6.5% residual contamination was present. This was the worst case. The ratio S was observed to be independent of bias in these circumstances. Further, precise calibration of the efficiency for electron detection was achieved by detecting the same scattered electron momentum at low q^2 and 31°. Here momentum resolution alone was sufficient to define an elastic electron. No additional error resulted from this high bias.

A further background was present from particles following spurious trajectories through the single stage of momentum resolution. These were measured by data taken 11% in momentum above the hydrogen elastic peak. After subtracting target wall and nonelectromagnetic backgrounds (where present) remaining counts were assumed due to this cause. They were measured to be weakly dependent on magnet current and were therefore directly subtracted from the hydrogen data. The same fractional background was subtracted from the deuterium data. In this subtraction procedure only statistical uncertainties were assigned. The ratio S

TABLE II. Fractional uncertainties in σ_{ed} relative to σ_{ep}.

Source	q^2 0.389 (BeV/c)^2	q^2 3.89 (BeV/c)^2
Counting statistics	0.016	0.055
Excess counts above peak	0.000	0.04
Inelastic contamination	0.000	(0.08)
Monitoring (fraction of bremsstrahlung and target wall corrections)	0.035	0.008
Momentum acceptance	0.03	0.03
Machine energy shifts	0.01	0.005
Total	0.05	0.075
Added in quadrature		(±0.116) if inelastics are subtracted

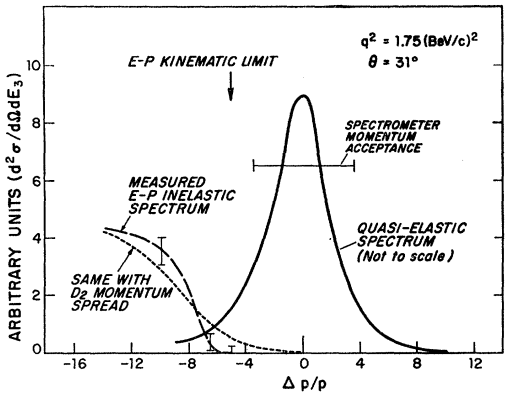

FIG. 4. Folding of inelastic e-p spectrum with momentum broadening due to deuteron wave function.

should not be influenced by the subtraction. The contamination varied from 0.000 at $q^2=0.389$ (BeV/c)^2 to 0.13 at $q^2=3.89$ (BeV/c)^2 and was typically 0.02.

Table II summarizes the sources of uncertainty present in two representative points. Below $q^2=2.92$ (BeV/c)^2 monitoring and momentum acceptance uncertainties dominate. Above this, statistical errors and ambiguities in the subtraction of inelastic backgrounds account for most of the uncertainties. The values and upper limits for S so derived, are given later in Table V. In addition to the error listed, theoretical uncertainties discussed in Appendix I may also be present. Note that with the electron-detection method these uncertainties are magnified by 3 to 4 when a value for R is derived.

III. ANTICOINCIDENCE METHOD

At momentum transfers between 0.389 and 1.17 (BeV/c)^2 and at forward angles it was possible simultaneously to measure S by the second method. A high-energy recoil proton was detected by a three-counter telescope (counters 1b, 2, and 3 in Fig. 5), the output of which was placed in fast coincidence ($2\tau=16$ nsec) with a pulse which signified that an electron had been detected within the 6.9% momentum interval. The solid angle subtended by the proton telescope was sufficiently large that less than 0.039 of the quasi-elastic protons recoiled at angles outside the telescope. This fraction

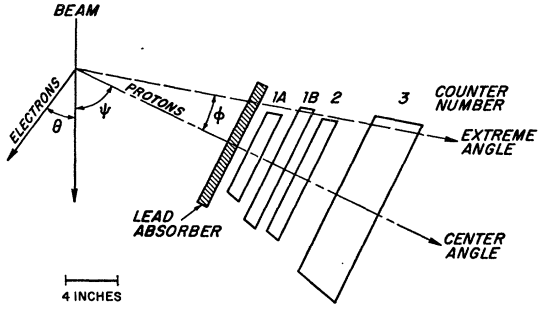

FIG. 5. Proton detection counter telescope.

TABLE III. Ratio of electron-proton elastic scattering cross section obtained from deuterium coincidence measurements to that obtained from hydrogen.

q^2 in (BeV/c)^2	σ_p from D_2/σ_p from H_2
0.389	0.958 (1±0.088)
0.623	1.02 (1±0.059)
0.857	1.042 (1±0.079)
1.17	1.035 (1±0.062)

varied from 0.039 at $q^2=0.389$ to 0.014 at $q^2=1.17$ (BeV/c)^2. Thus we obtain with a single measurement, with a deuterium target

$$S=\sigma_{en}/\sigma_{ep}$$

$$=\frac{\text{Electron arm counts}-\text{coincidence counts}}{\text{coincidence counts}}. \quad (5)$$

This technique reduced the importance of monitoring errors by a factor of 2 to 3 over the noncoincidence data. The statistical error is directly that of the difference in counts. To reduce background counting rates, lead absorber was placed in front of the proton telescope. The detection efficiency under these circumstances was measured for the center of these counters by detecting coincidences from electron-proton elastic scattering with hydrogen in the target. This detection efficiency ranged between 79% at $q^2=1.17$ (BeV/c)^2 to 88% at $q^2=0.389$ (BeV/c)^2. A correction of less than 1% was applied to this calibration to compensate for additional single and plural Coulomb scattering, elastic nuclear scattering, and additional nuclear absorption to be expected near the edge of the telescope.

Target wall backgrounds were subtracted using separate solid target data and the known fraction of bremsstrahlung from the target wall. Typically this correction was 3% of the counting rate in both the deuterium and hydrogen runs.

To obtain the ratio S, the neutron-to-proton conversion efficiency of the lead and scintillator to a point one-half way through counter No. 1b was needed. To estimate this quantity, the known total absorption cross section for each element was scaled by the factor Z/A.[12] The fraction of recoils detected by the telescope was

TABLE IV. Fraction of protons in 2° annulus between counters No. 1a and 1b.

q^2 (BeV/c)^2	Run	Total predicted	Total observed
0.389	1	0.072	0.084 1±0.1
0.389	2	0.049	0.035 1±0.15
0.623	1	0.047	0.057 1±0.15
0.857	1	0.029	0.030 1±0.20
1.17	1	0.028	0.03 1±0.2
1.17	2	0.029	0.037 1±0.2

[12] R. W. Williams, Rev. Mod. Phys. 36, 815 (1964).

TABLE V. Summary of σ_n/σ_p obtained from noncoincidence (*NC*) and coincidence (*C*) measurements. Neutron cross sections are also listed along with the assumed proton cross sections.

q^2 (BeV/c)^2	θ (degrees)	S_{NC}	$\Delta S_{NC}/S_{NC}$	S_C	$\Delta S_C/S_C$	$\bar{S}$	$\Delta\bar{S}/S$	$\sigma_p\times10^{32}$ (cm^2)	$\Delta\sigma_p/\sigma_p$	$\sigma_n\times10^{32}$ (cm^2)	$\Delta\sigma_n/\sigma_n$
0.389	40.6	0.375	0.24	0.387	0.085	0.385	0.081	7.67[a]	0.03	2.92	0.097
0.623	31	0.438	0.170	0.411	0.12	0.421	0.095	4.92[a]	0.035	2.07	0.104
0.857	31	0.424	0.21	0.368	0.11	0.380	0.092	2.28[a]	0.06	0.847	0.108
1.17	31	0.390	0.160	0.367	0.118	0.376	0.088	0.903	0.065	0.340	0.11
1.17	90	0.499	0.175	···	···	···	···	0.0711	0.062	0.0355	0.180
1.75	31	0.567	0.20	···	···	···	···	0.246	0.07	0.0139	0.21
1.75	90	0.687	0.22	···	···	···	···	0.0163	0.073	0.0112	0.225
2.92	31	0.55	0.21	···	···	···	···	0.0360	0.057	0.0198	0.215
3.89	31	<0.707	0.22	···	···	···	···	0.0100	0.07	0.00707	0.23
6.81	41.9	<0.40	1.30	···	···	···	···	0.00058	0.21	0.00023	1.32

[a] From Janssens, Ref. 14.

estimated using the angular distribution for n-p charge exchange scattering.[13] The correction estimated in this manner was typically 2% and always less than 3.1%. An uncertainty of $\frac{1}{2}$ of the correction was assigned.

The incident beam intensity was limited by counting rate effects in the proton arm. The dependence on rate was directly measured by varying the incident beam current and observing the change in the coincidence counting rate. The beam intensity was adjusted until there was less than 0.5% variation from the low beam coincidence rate.

Two methods were used to check the over-all reliability of the anticoincidence method. Firstly, the electron-proton elastic-scattering cross section derived from data taken with deuterium in the target was compared with the same cross section measured with hydrogen in the target. These numbers should agree if the impulse approximation is valid. As shown in Fig. 6 and Table III, they are seen to agree within the 7% precision of the comparison. All radiative corrections have been included. At $q^2=0.389$ and 0.623 (BeV/c)^2 the final-state corrections of Nuttall and Whippman[11] were applied to the noncoincidence counting rate before making the comparison. A simple calculation shows that this implies that the ratios S are reliable to at least 25% precision.

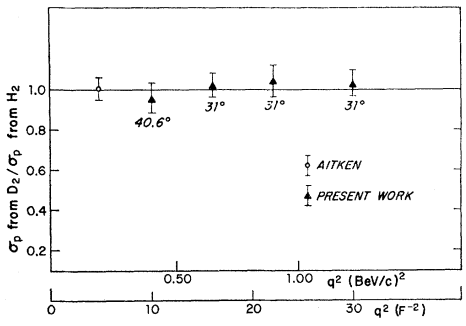

FIG. 6. A comparison between $d\sigma/d\Omega_{ep}$ derived from the deuteron coincidence data and the cross section obtained with hydrogen in the target.

[13] V. Z. Dzhelepov, B. M. Golovin, M. Kazarinov, and N. H. Semenov, 1956 CERN Conference Report, p. 115.

The check is less accurate than the data. We assume the data are in fact more reliable than this.

Secondly, the coincidence counting rate was simultaneously measured at two solid angles differing by 50%. The electronic circuits were arranged so that particles missing counter No. 1a but triggering the remainder of the proton telescope (counters 1b, 2, and 3 in Fig. 5) were directly recorded. The number of protons to be expected in this angular region was also calculated as a fraction of the total rate. Approximately 70% of the counts come from the impulse approximation and angular distribution and 30% arises from multiple scattering and the neutron-to-proton conversion efficiency of the counters. Table IV shows the observed fraction of protons to be consistent with calculations. We were encouraged, but attach only qualitative significance to these numbers. In particular, the limits placed by this measurement on a possible breakdown of the impulse approximation are not clear to us. The number of particles in the region is not large and depends more on the high momentum components of the deuteron wave function.

Both the coincidence and noncoincidence ratios are listed in Table V. Only experimental uncertainties are included. Since the two measurements are statistically independent, they were averaged to obtain a better value for R. To extract the electron-neutron scattering cross section we prefer to use consistently the precise

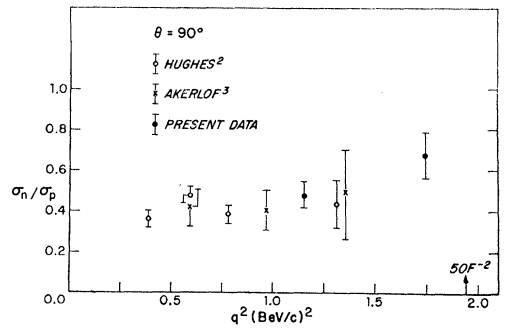

FIG. 7. $S=\sigma_n/\sigma_p$ for $\theta=90°$ scattering. (Comparable data from other laboratories are shown for comparison.)

TABLE VI. Neutron form factors.

q^2 (BeV/c)^2	G_{Mn}/μ_n	$\Delta G_{Mn}/\mu_n$	G_{En}^2	ΔG_{En}^2	$(\tau G_{Mn})^2$	No. of points	χ^2	Data used
0.389	0.445	0.021	+0.026	0.014	0.0078	10	26.3	Hughes-Harvard
0.389	0.445	0.017	−0.034	0.012	0.0078	9	6.0	Hughes
0.623	0.310	0.021	+0.007	0.014	0.011	6	7.2	Hughes-Harvard
0.857	0.218	0.028	+0.007	0.015	0.010	2	0	Hughes-Harvard
1.17	0.177	0.014	−0.009	0.009	0.012	4	0.14	Hughes-Harvard
1.17	0.183	0.021	−0.012	0.013	0.013	2	0	Harvard
1.75	0.120	0.011	−0.003	0.012	0.011	2	0	Harvard
2.92	$\leqslant$0.052	0.005	$\leqslant$0.102	0.02	...	...	...	Harvard
3.89	$\leqslant$0.036	0.007	$\leqslant$0.0066	0.0015	...	...	...	Harvard
6.81	$\leqslant$0.014	+0.006 −0.013	...	...	...	...	...	Harvard

measurements of the electron-proton scattering cross section by Janssens[14,15] where available.

Comparison with Data of Other Laboratories

The present 90° measurements overlap the data of Hughes *et al.*,[2] and of Akerlof *et al.*,[3] at $q^2=1.17$ (BeV/c)^2. These ratios are plotted in Fig. 7 where the agreement between these sets is shown to be within the rather large uncertainties involved. However, at $q^2=0.389$ (BeV/c)^2 and 40.6° the present measurements yield a value for S of 0.382±0.03. This number is somewhat higher than would be obtained by extrapolation of either Stanford data[2] [where $S=0.179\pm0.031$ at $q^2=0.389$ (BeV/c)^2 and $\theta=45°$] or the coincidence measurements of Stein *et al.* (where $S=0.26\pm0.04$ at the same q^2 at 50° scattering angle[4]). In Fig. 8 we plot S for the forward-angle data taken in the present experiment.

IV. SUMMARY OF EXPERIMENTAL RESULTS

The cross sections for electron-neutron scattering were observed to be less than that for electron-proton scattering at all momentum transfers and scattering angles investigated. This was true even at the two highest momentum transfers where the data were almost certainly contaminated with electrons from inelastic processes.

Upper Limits to the Neutron Form Factors at $q^2=2.92$ (BeV/c)^2 and Above

Data at only one scattering angle were obtained in this region and upper limits on the form factors were derived by alternately attributing the entire cross section to one or the other form factor. As can be seen from Table VI the $q^2=6.81$ (BeV/c)^2 data yields, $G_{Mn}=0.024_{-0.024}{}^{+0.012}$. This is the smallest form factor measured. The most stringent limits on G_{En} were obtained from the $q^2=3.89$ (BeV/c)^2 point where $G_{En}=0.081\pm0.009$ and errors are standard deviations.

[14] T. Janssens, thesis, Stanford University, 1964 (unpublished).
[15] D. W. Aitkin, *Proceedings of the International Conference on Nucleon Structure*, edited by R. Hofstadter and L. I. Schiff (Stanford University Press, Stanford, California, 1963), p. 336.

The form factors are observed to decrease with increasing momentum transfer. A $1/q^2$ dependence, to be expected from a resonance model without "core terms," is consistent with the data.[6] So are more rapid dependences on momentum transfer. In any event, the above numbers are upper limits on such "core terms."

Neutron Form Factors at $q^2=0.389$ to 1.75 (BeV/c)^2

Form factors have been extracted from the cross-section data, using a least-squares fitting program to an equation of the form

$$y=mx+b \text{ (with only } y \text{ liable to error)},$$

$$y=\frac{\sigma_{\text{expt}}}{\sigma_{\text{Mott}}}[\cot^2(\theta/2)](1+\tau), \qquad (6)$$

$$x=\cot^2(\theta/2), \quad \tau=q^2/4m^2.$$

The slope m is proportional to the quantity $(G_E^2+\tau G_M^2)$ whereas the intercept b is proportional to G_M^2 alone. This procedure is discussed in I. It should be noted that the uncertainties in G_E and G_M are almost completely correlated.

To effect the form-factor separation at $q^2=0.389$, 0.623, and 0.857 (BeV/c)^2, the present measurements were combined with the more backward-angle ratio data of Hughes *et al.*[2] In all cases the proton form factors of

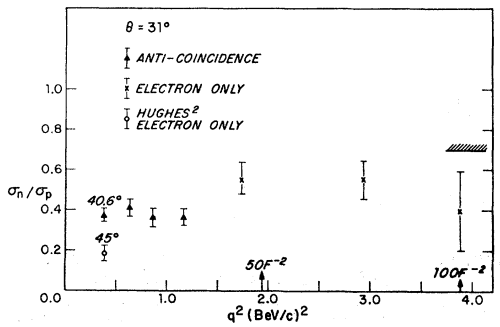

FIG. 8. $S=\sigma_n/\sigma_p$ for $\theta=31°$ scattering.

TABLE VII. Comparison of proton and neutron form factors.

q^2 (BeV/c)^2	G_{Ep}	ΔG_{Ep}	G_{Mp}/μ_p	$\Delta G_{Mp}/\mu_p$	G_{Mn}/μ_n	$\Delta G_{Mn}/\mu_n$	$(1+q^2/0.71)^{-2}$	Proton data used	Neutron data used
0.389	0.424	0.017	0.409	0.007	0.445	0.021	0.418	Janssens	Hughes Harvard
0.623	0.281	0.024	0.286	0.006	0.310	0.023	0.284	Janssens	Hughes Harvard
0.857	0.183	+0.026 −0.034	0.228	0.005	0.218	0.028	0.205	Janssens Chen	Hughes Harvard
1.17	0.17	+0.02 −0.03	0.155	0.004	0.177	0.014	0.143	Janssens Chen	Hughes Harvard
1.75	0.114	+0.022 −0.029	0.0895	0.005	0.120	0.021	0.084	Berkelman Chen	Harvard
2.92	0.00	+0.04	0.049	0.006	$\leqslant$0.052	0.005	0.038	Chen	Harvard
3.89	0.00	+0.02	0.0325	0.0033	$\leqslant$0.036	0.007	0.024	Chen	Harvard

Janssens were used to compute the electron-proton scattering cross sections.[16]

At $q^2=1.17$ (BeV/c)^2 Harvard electron-proton cross sections were used. At $q^2=1.75$ (BeV/c)^2 only the present measurements were available. Representative linear separations of $(G_E^2+\tau G_M^2)$ and G_M^2 are shown in Fig. 9. The sensitivity of the slope m to the present data is evident. The results of several combinations of data are listed in Table VI. In Fig. 10 the Hughes and Harvard data are plotted. We plot the square of G_{En} since the interpretation of the error flags is more transparent.

Phenomenological Relations and Form Factor Fitting

The extent to which

$$G_{Ep}=G_{Mp}/\mu_n=G_{Mn}/\mu_n=(1+q^2/0.71)^{-2} \qquad (7)$$

is shown in Fig. 11 and in Table VII.[16] These relations are consistent with the data out to the highest momentum transfer measured [$q^2=6.81$ (BeV/c)^2]. They suggest that a one-parameter model can describe the data. The apparent exponential dependence may be fortuitous.

At the same time Table VI indicates that the speculation $G_{En}^2=(\tau G_{Mn})^2$ is not particularly well tested by the present data because of the errors present. The values for G_{En}^2 at $q^2=0.389$ (BeV/c)^2 appear somewhat high. In view of the necessity for using the data from different laboratories to obtain form factors, we do not regard the value of G_{En}^2 as determined by this data. However, the coincidence measurements appear capable of at least 10 times higher experimental precision than was achieved. This increased sensitivity could be used to study G_{En}^2.

Details of attempts to understand this data theoretically are presented in an accompanying paper.

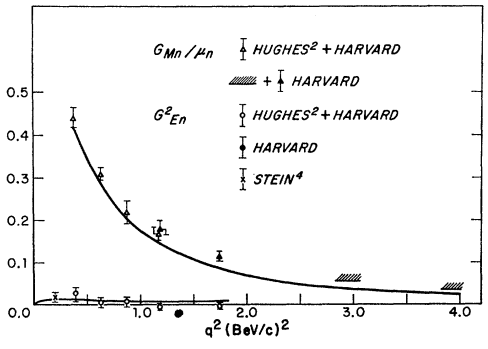

FIG. 9. Neutron electromagnetic form factors. Curves are from Eqs. (2) and (7) of text.

[16] An $SU(6)$-invariant model predicts $G_{Mn}/\mu_n=G_{Mp}/\mu_p$. K. J. Barnes, P. Carruthers, and Frank von Hippel, Phys. Rev. Letters **14**, 82 (1965).

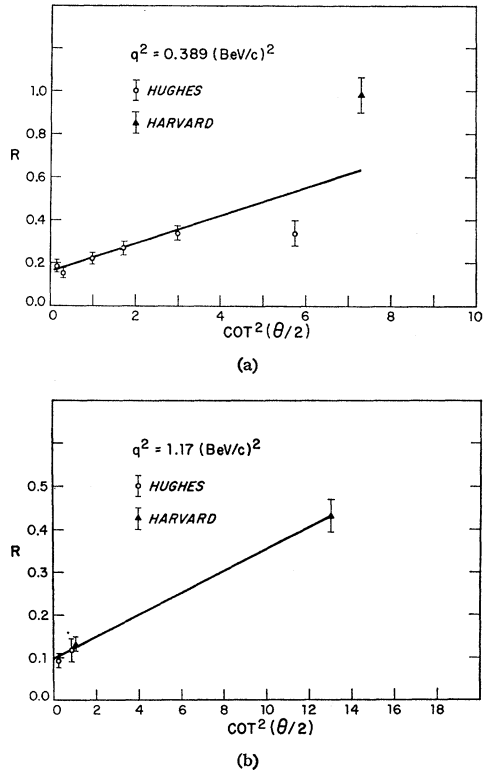

FIG. 10. Graphs showing reduced experimental cross section versus $\cot^2(\theta/2)$. Solid line is least-squares fit to all of data, assuming linear dependence $R=\sigma_{\text{exp}}/\sigma_{\text{Mott}}\times(1+\tau)\cot^2(\theta/2)$.

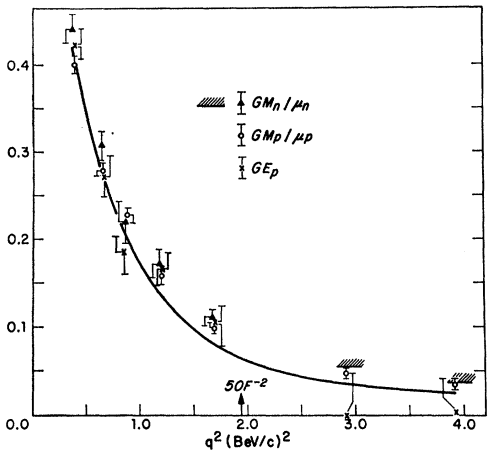

FIG. 11. Graph showing experimental test of relation $G_{Ep}=G_{Mp}/\mu_p=G_{Mn}/\mu_n$. The curve is Eq. (7) of text.

ACKNOWLEDGMENTS

These experiments were conducted with the cooperation and assistance of the personnel of the Cambridge Electron Accelerator and Cyclotron Laboratory.

Dr. Hugh Jones and Dr. R. Atkinson and Professor L. Durand provided helpful advice concerning the analysis.

APPENDIX

The elastic electron-neutron scattering cross section must be extracted from the observed quasi-elastic scattering. Many details of the theoretical analysis used for the present data are described here. It is hoped this information will be of use to those wishing a further understanding of the sources of uncertainty.

The impulse approximation was used to compute the fraction of electrons scattered quasi-elastically within the momentum acceptance of the spectrometer. It was also used to calculate the fraction of recoil protons associated with these quasi-elastic electrons which were missed by the proton telescope. For the case of electron detection and S-state scattering we have from Durand[9]:

$$\frac{d^2\sigma_d}{d\Omega dE_3}=\frac{M_m^2 E_1 p_{\text{c.m.}}}{\pi\, E_3 E_{\text{c.m.}}}\left[\frac{d\sigma_p}{d\Omega}\mathfrak{M}_p(p,q)+\frac{d\sigma_n}{d\Omega}\mathfrak{M}_n(p,q)\right], \quad \text{(A1)}$$

where

M_m = mean of proton and neutron masses,

$p^2=p_{\text{c.m.}}^2=M_m q_0-\frac{1}{4}q^2$,

E_1 = incident electron energy,

$E_{\text{c.m.}}^2=p_{\text{c.m.}}^2+M_m^2$,

and

E_3 = final electron energy.

The integral under the quasi-elastic peak is nearly the sum of free electron-proton and free electron-neutron scattering

$$\int_0^{E_{3\max}}\frac{d^2\sigma_d}{d\Omega dE_3}dE_3=(\sigma_{ep}+\sigma_{en})(1+\Delta)=\sigma_{ed}. \quad \text{(A2)}$$

The quantity Δ arises from a kinematic weighing of lower momentum transfers. For the present experiment it ranged from +0.01 to +0.02. The form-factor variation across the portion of the quasi-elastic peak studied cancels to first order.

In Eq. (A1), the electron is treated relativistically and is regarded as interacting with one or the other of the two nucleons. The current operator for a bound nucleon in the deuteron is assumed to be that of a free nucleon.

By observed quasi-elastic events we are selecting out the long-range or low-momentum components of the deuteron wave function. The momentum transfers considered here are assumed large by comparison with the momentum associated with the deuteron binding energy ($\sim$40 MeV/c). The accuracy of an impulse approximation calculation depends on these assumptions and two parameters of the wave function derived from low-energy experiments.[17] The binding energy of the deuteron determines α. The triplet effective range determines β. These quantities are in turn known to high precision from such work.

Initially, the two nucleons have a momentum distribution with respect to each other which is given, at least in the nonrelativistic approximation, by the Fourier transformation of the deuteron wave function. The function $\mathfrak{M}(p,q)$ in Eq. (A1), expresses the effects of this moving target on the momentum distribution of the scattered electrons.

Two models for the deuteron ground-state wave function were used to calculate $\mathfrak{M}(p,q)$. In the one model chosen to analyze the data, both the Hulthén[18] and an approximate repulsive-core wave function were compared. The repulsive-core model was used. D-state contributions were calculated assuming a 6.5% D-state probability.

Form of $\mathfrak{M}(p,q)$

A partially covarient form of the momentum distribution of recoil particles[9] was used to compute both the spectrum of scattered electrons and the angular distribution of the recoil protons. Here relativistically correct kinematics were used, and the Fourier transform was performed in the reference frame where $q_0=0$ at the quasi-elastic peak. Following Durand,

$$\mathfrak{M}_p(p,q)=\frac{1}{2}\int_0^{\pi}F^2(\varphi)d\cos\varphi,$$
$$\mathfrak{M}_n(p,q)=\frac{1}{2}\int_0^{\pi}F^2(\pi-\varphi)d\cos\varphi, \quad \text{(A3)}$$

[17] Richard Wilson, *The Nucleon-Nucleon Interaction* (Interscience Publishers, Inc., New York, 1963).

[18] L. Hulthén and M. Sugawara, *Handbook of Physics*, edited by S. Flügge (Springer-Verlag, Berlin, 1957), Vol. 39.

and

$$F(\varphi)=N\int_0^\infty j_0(kr)u(r)rdr,$$

$$k=\left[\left[\frac{|\mathbf{q}|}{2}-\frac{M_D+q_0}{2E_{\text{c.m.}}}p_{\text{c.m.}}\cos\varphi_{\text{c.m.}}\right]^2+p_{\text{c.m.}}{}^2\sin^2\varphi_{\text{c.m.}}\right]^{1/2}. \quad \text{(A4)}$$

The quantity k is the momentum of the spectator neutron in the laboratory frame of reference. The angle φ is the nucleon recoil angle in the $q_0=0$ reference frame. $F(\pi-\varphi)$ refers to the spectator proton.

For completeness

$$\begin{aligned} q^2&=4E_1E_3\sin^2(\theta/2),\\ E_{3\text{ peak}}&=(E_1-b)/1+2(E_1/M_m)\sin^2(\theta/2),\\ q_0&=E_1-E_3-b,\\ |\mathbf{q}|^2&=q^2+q_0{}^2,\\ b&=0.0022245\text{ BeV}. \end{aligned} \quad \text{(A5)}$$

When the integration over the nucleon recoil angle is performed, both the proton and neutron cases reduce to the same expression; that is, $\mathfrak{M}_n(p,q)=\mathfrak{M}_p(p,q)$. When the recoil proton was detected this integration was omitted and the now triply differential cross section transformed into the laboratory frame using

$$\tan\varphi_{p\text{lab}}=\frac{p_{\text{c.m.}}\sin\varphi_{\text{c.m.}}}{\frac{1}{2}|\mathbf{q}|+[(m_D+q_0)/2E_{\text{c.m.}}]p_{\text{c.m.}}\cos\varphi_{\text{c.m.}}}. \quad \text{(A6)}$$

The second form of $\mathfrak{M}(p,q)$ considered was the result of a dispersion-theory calculation of Durand.[9] He found

$$\mathfrak{M}(p,q)=\frac{N^2}{p|\mathbf{q}_d|^2}\left[(x^2-1)^{-1}+(y^2-1)^{-1}-\frac{1}{y-x}\ln\left[\frac{(x+1)(y-1)}{(x-1)(y+1)}\right]\right], \quad \text{(A7)}$$

$$|\mathbf{q}_d|^2=q^2+[\tfrac{1}{4}q^2-p^2-\alpha^2]^2/(M_m{}^2+p^2),$$

$$x=\frac{\alpha^2+p^2+\frac{1}{4}q^2}{p|\mathbf{q}_d|},\quad y=\frac{\beta_H{}^2+p^2+\frac{1}{4}q^2}{p|\mathbf{q}_d|}.$$

In both these equations the deuteron ground-state wave function is given by

$$\psi(r)=\frac{N}{(4\pi)^{1/2}}\frac{u(r)}{(r)}. \quad \text{(A8)}$$

For the Hulthén model,[18] which is used specifically in (A7)

$$\begin{aligned} u(r)&=\cos\epsilon[e^{-\alpha r}-e^{-\beta_H r}],\\ \alpha&=0.2317,\\ \beta_H&=1.389\pm0.007,\\ \cos\epsilon&=0.9991=\text{mixing parameter}. \end{aligned} \quad \text{(A9)}$$

These two calculations of $\mathfrak{M}(p,q)$ were compared using the same parameters for the Hulthén wave function. As can be seen from Table VIII, the fraction of particles with the momentum acceptance of the electron spectrometer is identical for the two calculations to 0.3%. However, the over-all normalization of (A7) is higher than that of (A3) by 1.4%. This normalization shift was also noted by Nuttall and Whippman.[11] Further, the dispersion-theory approach [Eq. (A7)] predicts about 5% more scattering on the low-momentum side and about 5% less scattering on the high-momentum side of the quasi-elastic peak. Since the momentum acceptance of the spectrometer is symmetric about the peak, this has little effect on the experimental result.

These ambiguities are a factor of 3 less than the most precise cross sections measured. The first form for $\mathfrak{M}(p,q)$ was chosen to reduce the data because of the ease with which a more refined wave function could be introduced and the angular distribution of recoil protons computed.

In both approximations the shape of the quasi-elastic peak depends only on the scattering angle and is independent of momentum transfer in the range considered. This is a result of the relativistic kinematics and not due to the details of the deuteron wave function used.

Choice of S-State Wave Function

For all wave functions used, the normalization was chosen so that

$$N^2\int_0^\infty u^2(r)dr=1.0. \quad \text{(A10)}$$

Or if both s and d waves were considered, then

$$N^2\int_0^\infty [u^2(r)+w^2(r)]dr=1.0. \quad \text{(A11)}$$

The quantity N^2 was determined by the triplet effective range ρ_t[17]:

$$\begin{aligned} N^2&=2\alpha/(1-\alpha\rho_t)=0.7769[1\pm0.003],\\ \rho_t&=\rho_{0t}+2\alpha\rho_{0t}{}^2\rho_t',\quad \rho_{0t}=1.732[1\pm0.007]\times10^{13},\\ \rho_t'&=0.017\pm0.013. \end{aligned} \quad \text{(A12)}$$

The S-state wave function chosen to interpret the data was approximation II of Moravcsik[19]:

$$\begin{aligned} u(r)&=(1-e^{-\beta r})(e^{-\alpha r}-e^{-\beta r})\cos\epsilon,\\ \beta&=1.874\pm0.007. \end{aligned} \quad \text{(A13)}$$

Table VIII shows that use of Eq. (A13) in preference to the Hulthén wave function changes the fraction of particles within the momentum acceptance by only 1.4%. The uncertainty in the parameters of the deuteron wave function, a and β, was found to introduce about 0.3% uncertainty in the deuterium cross section.

[19] M. J. Moravcsik, Nucl. Phys. 7, 113 (1958).

TABLE VIII. Comparison of deuteron wave functions and models at $q^2=1.75$ (BeV/c)^2 and 31°.

$\mathfrak{M}(p,q)$ Equation No.	Wave function equation	$\left(\frac{d\sigma_d}{d\Omega}\right)\times10^{31}$ [a] (cm^2/sr)	$\left(\frac{d^2\sigma_d}{d\Omega dE_3}\right)_{\text{peak}}\times10^{33}$ [a] (cm^2/sr MeV)	Fraction of scattering in momentum acceptance
(A4)	Repulsive core	0.7835	0.653	0.749
(A4)	Hulthén	0.7829	0.647	0.741
(A7)	Hulthén	0.7952	0.658	0.743
	Elastic scattering	0.7820	...	1.000
	Computational uncertainty	±0.2%	±0.35%	±0.3%

[a] Unity form factors.

D-State Scattering

The momentum distribution of electrons scattering from the D state is broader than that from the S state. Thus the net effect will be to decrease the fraction of particles within the momentum acceptance of the spectrometer. Following Durand,[20] the approximate cross section

$$\frac{d^2\sigma_d}{d\Omega dE_3}=\sigma_{\text{Mott}}\frac{M_m^2}{2\pi}\frac{P_{\text{c.m.}}}{E_{\text{c.m.}}}\Big\{[A'G_{En}^2+B'G_{Mn}^2]\times\int_0^\pi (F^2(\pi-\varphi)+G^2(\pi-\varphi))d\cos\varphi+[A'G_{Ep}^2+B'G_{Mp}^2]$$
$$\times\int_0^\pi (F^2(\varphi)+G^2(\varphi))d\cos\varphi+\frac{q^2}{2M_m^2}G_{Ep}G_{Mn}\int_0^\pi [-G(\varphi)G(\pi-\varphi)+F(\varphi)F(\pi-\varphi)]d\cos\varphi$$
$$+\tfrac{2}{3}\frac{q^2}{4M_m^2}G_{Mn}G_{Mp}[2\tan^2(\theta/2)+1]\int_0^\pi (\sqrt{2}F(\varphi)G(\pi-\varphi)+\sqrt{2}F(\pi-\varphi)G(\varphi)$$
$$+G(\varphi)G(\pi-\varphi)+F(\varphi)F(\pi-\varphi))d\cos\varphi\Big\}, \quad \text{(A14)}$$

where $G(\varphi)=N\int_0^\infty j_2(kr)w(r)rdr$ was used to compute this scattering.

The function $G(\varphi)$ is similar to a Fourier transform. To evaluate this we have used Hulthén's two-parameter D-state wave function which he evaluates for a 5% D-state probability

$$w(r)=\sin\epsilon K^2e^{-\alpha r}[1+3K/\alpha r+3K^2/(\alpha r)^2], \quad \text{(A15)}$$

where

$$K=[1-e^{-\alpha\mu' r}], \quad \mu'=3.28, \quad \sin\epsilon=0.0275.$$

The result was then scaled to a 6.5% probability. The S-state wave function was renormalized to 0.935. The functions $G(\varphi)$ and $F(\pi-\varphi)$ are nearly orthogonal, and the main contributions come from the $G^2(\varphi)$ terms. Tables IX and X and Fig. 12 indicate the nature of the result. Note that the change in S-state normalization affects mainly the parameter beta. However, the scattering we are concerned with is most sensitive to the binding energy parameter α. At the peak the electron scattering is reduced by only 0.6 of the change in normalization. Taking these factors into account, a uniform 3% correction was applied to the electron arm data. When the recoil proton was detected in coincidence with the electron, only the portion of the D-state which was counted by the electron arm need be considered. This entered as a 1% correction to the coincidence data.

The major problem in this is the large uncertainty in the 6.5% figure for the D-state probability. Presently it depends on calculation rather than on measurement.[17]

TABLE IX. D-state corrections to the scattering for $P_D=6.5\%$. All are fractional corrections.

q^2 (BeV/c)^2	θ (degrees)	S-state loss from new normalization	Recovered from G^2 term	Lost in interference terms	Total loss from 6.94% momentum acceptance
0.384	40.6	−0.036	+0.014	−0.008	−0.032
1.17	31	−0.036	+0.014	−0.005	−0.027
1.17	90	−0.036	+0.014	−0.005	−0.027

[20] L. Durand, III, Phys. Rev. **115**, 1020 (1959).

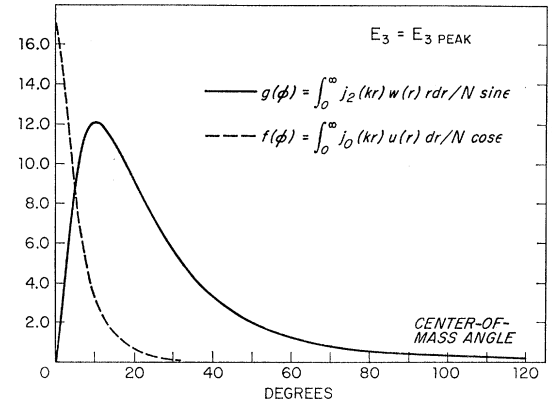

FIG. 12. Curves showing extent to which $f(\varphi)$ and $g(\varphi)$ are orthogonal at $q^2=1.17$ (BeV/c)^2 and $\theta=31°$. The function $f(\varphi)$ is formed from $F(\varphi)$ defined in Eq. (A4) by removing the normalization factor $N\cos\epsilon$. Similarly the function $g(\varphi)$ differs from $G(\varphi)$ in Eq. (A14) by the normalization factor $N\sin\epsilon$.

Final-State Correction

Final-state effects were included at $q^2=0.389$ and 0.623 (BeV/c)^2 using the calculation of Nuttall and Whippman. For higher momentum transfers they have not been calculated. Jones[21] finds that the contribution of the square diagram shown in Fig. 13(a) decreases as m_π^2/q^2 relative to the impulse approximation diagram 13(b). The effects were therefore neglected in the present analysis. Where included, the final-state effect corrections raise the deuteron cross section by 1.5–1.8%. For q^2 below 0.389 (BeV/c)^2 the correction becomes more important.

No final-state corrections were applied to the anticoincidence data. That portion of the final-state interaction which is symmetric between neutron and proton will cancel in this case. Any residual corrections remain in the data.

By way of summary the estimated uncertainties in the deuterium cross section are given in Table XI. For the case of $q^2=1.17$ (BeV/c)^2 the resultant uncertainty in the neutron cross section is indicated on the fraction of the scattering from the neutron. It is seen that the coincidence measurements are a factor of 3 less sensitive to these considerations than are the noncoincidence measurements.

TABLE X. Coincidence corrections for D-state scattering detected by electron arm but missed by proton telescope.

q^2 (BeV/c)^2	θ (degrees)	S-state loss from new normalization
0.389	40.6	0.007
0.389	40.6	0.006 (second run)
0.623–1.17	31	0.006

[21] H. F. Jones, thesis, Imperial College, London, 1963 (unpublished).

TABLE XI. Estimate of theoretical uncertainties in the electron-detection and anticoincidence measurements.

Source	Fractional error in σ_d	Fractional error in σ_n/σ_p for $q^2=1.76$ (BeV/c)^2 $\theta=31°$
Electron detection		
Choice of $\mathfrak{M}(p,q)$	0.013	0.043
Choice of repulsive-core wave function	0.007	0.023
S-state parameters	0.003	0.010
−3% uncertainty in d-state probability	−0.015	−0.049
Omission of final-state interactions	?	?
If added in quadruture	0.021	0.072
Experimental uncertainty momentum acceptance	0.025	0.083
Anticoincidence		
	Fractional error in R, $q^2=1.17$ (BeV/c)^2 and $\theta=31°$	
Choice of $\mathfrak{M}(p,q)$	0.004	
Choice of repulsive-core wave function	0.004	
S-state parameters	0.001	
−3% in d state	−0.005	
If added in quadruture	0.008	
Experimental uncertainties in R.	+0.028	

Radiative Corrections

Before interpreting the observed cross-section data in terms of the single-photon-exchange diagram, radiative corrections for bremsstrahlung from both the electron and proton lines were applied to the data.

The radiative corrections for elastic electron-proton scattering were taken from Meister and Yennie[22] and are discussed in Paper I.

The radiative corrections to the quasi-elastic continuum of deuterium were calculated from Meister and Griffy.[10] They computed the case of electron radiation only. To allow for radiation by the proton line, the

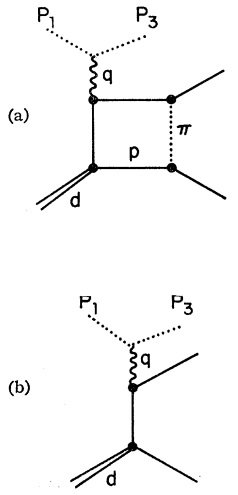

FIG. 13. Feynman diagram of possible final-state interactions. (a) Possible final-state interaction. (b) Quasi-elastic scattering.

[22] N. T. Metiser and D. R. Yennie, Phys. Rev. **130**, 1210 (1963).

TABLE XII. Hydrogen corrections.

q^2 (BeV/c)^2	θ (degrees)	δ_{I}	δ_{II}	δ_{III}	$\delta_{\mathrm{hydrogen}}$
1.17	31	0.153	0.011	0.0015	0.1655
1.17	90	0.138	0.027	0.002	0.167
3.89	31	0.157	0.021	0.006	0.184

appropriate electron-proton radiative correction terms were used to scale the answer upward by the factor $(1+\frac{2}{3}\delta_{\mathrm{II}}/\delta_{\mathrm{I}})$. The factor $\frac{2}{3}$ represents the approximate portion of the scattering from the proton in the deuteron. The quantity δ_{I} represents the correction due to bremsstrahlung from the electron line only. The quantity δ_{II} arises from the interference between the amplitude for radiation by the electron and proton lines. Here also the total correction was exponentiated. The effect of this correction on the deuterium spectrum is seen in Fig. 14 and is listed in Tables XII and XIII. In the case of deuterium, the correction is approximately constant with angle, whereas in the case of hydrogen, the correction is approximately constant with momentum transfer.

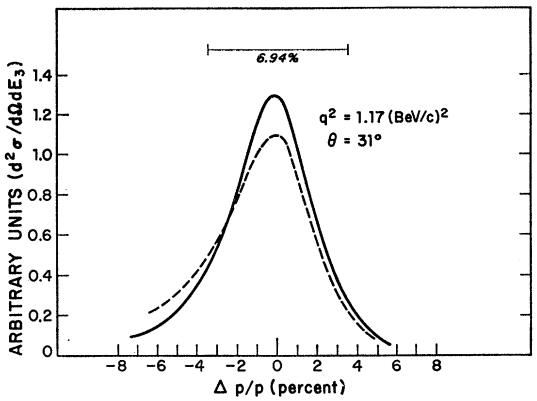

FIG. 14. Radiative corrections to quasielastic spectrum at $q^2=1.17$ (BeV/c)^2 and $\theta=31°$. Solid line is uncorrected S-state spectrum, dashed line is corrected spectrum.

Several calculational details are worth mentioning for those wishing to redo these computations. Meister and Griffy[10] split the calculation into hard- and soft-photon contributions and introduce a cutoff ΔE to separate them. They found

$$\delta_{\mathrm{soft}}=-\frac{\alpha}{\pi}\left[\ln\frac{\Delta E^2}{E_1E_3}\left[\ln\frac{q^2}{m_e^2}-1\right]-\tfrac{1}{2}\ln^2\left(\frac{E_1}{E_3}\right)+\frac{13}{6}\ln\frac{q^2}{m_e^2}-\frac{28}{9}\right],$$

$$\delta_{\mathrm{hard}}=\frac{\alpha}{\pi}\frac{1}{I(q^2)\mathfrak{M}(p,q)}\left\{\left[\int_{\Delta E}^{k_{\max i}}\frac{dk}{(1-k/E_1)^2}I(q_i)^2\times\frac{p_i}{E_{\mathrm{c.m.}i}}\mathfrak{M}(p_i,q_i)\times\left(\frac{1}{k}\left(1-\frac{k}{E_1}\right)\left(2\ln\frac{2E_1}{M}-1\right)+\frac{k}{E_1^2}\ln\frac{2E_1}{M}\right)\right]\right.$$
$$\left.+\left[\int_{\Delta E}^{k_{\max f}}\frac{dk}{[1-(k/E_3)]^2}I(q_f^2)\times\frac{p_f}{E_{\mathrm{c.m.}f}}\mathfrak{M}(p_f,q_f)\times\left(\frac{1}{k}\left(1+\frac{k}{E_3}\right)\left(2\ln\frac{2E_3}{M}-1\right)+\frac{k}{E_3^2}\frac{2E_3}{M}\right)\right]\right\},\quad\text{(A16)}$$

where

k = energy of emitted photon,

$q_i^2=q^2[1-(k/E_i)]$,

$q_f^2=q^2[1+(k/E_f)]$,

$\mathfrak{M}(p,q)$ as defined in Eq. (A3),

$$I(q^2)=\frac{1}{1+\tau}[G_{En}^2(q^2)+G_{Ep}^2(q^2)]+\left[\frac{\tau}{1+\tau}+2\tau\tan^2(\theta/2)\right][G_{Mn}^2(q^2)+G_{Mp}^2(q^2)].$$

TABLE XIII. Deuteron corrections.

q^2 (BeV/c)^2	θ (degrees)	Peak correction: δ_d, electron only	Peak correction: $[1+\frac{2}{3}(\delta_{\mathrm{II}}/\delta_{\mathrm{I}})]$	δ_d, total peak	Weighted average[a] δ_d
1.17	31	0.158	1.048	0.166	0.139
1.17	90	0.103	1.13	0.117	0.107
3.89	31	0.171	1.089	0.187	0.165

[a] Average over quasi-elastic spectrum within momentum acceptance.

$k_{\max}$ is determined by setting the three momenta for the recoiling nucleons in their own center-of-mass system equal to zero.

$$p_i^2=-\tfrac{1}{4}q_i^2+M(E_i-E_f-k_{\max i}-b)=0,$$
$$p_f^2=-\tfrac{1}{4}q_f^2+M(E_i-E_f-k_{\max f}-b)=0.\quad\text{(A17)}$$

The cutoff ΔE was chosen to give the correction a stable value which turns out to be a maximum. In the present case a ΔE of 10 MeV was used for the 90° measurements and the correction for q^2 below 0.9 (BeV/c)^2, whereas ΔE for 30 MeV was necessary for q^2 greater than 1.75 (BeV/c)^2. Typically a 10% difference in the correction factor was incurred by changing ΔE by 50% of its value.

Anticoincidence Radiative Corrections

The additional radiative correction incurred at $q^2=1.17$ (BeV/c)^2 and 31° by detecting the recoil proton in coincidence with the scattered electron with 40% momentum acceptance is 0.6% for elastic scattering. This factor cancelled out when the proton detection efficiency was measured with hydrogen in the target. No additional corrections were applied to the deuterium data.